Available online at www.sciencedirect.com
ScienceDirect
Polymer 47 (2006) 7835–7845
polymer
www.elsevier.com/locate/polymer

Molecular simulations of gas transport in nitrile rubber and styrene butadiene rubber

Esra Kucukpinar, Pemra Doruker*

Department of Chemical Engineering and Polymer Research Center, Bogazici University, Bebek 34342, Istanbul, Turkey

Received 11 April 2006; received in revised form 23 August 2006; accepted 24 August 2006
Available online 25 September 2006

Abstract

Nitrile rubber (NBR, 39:61 wt% of acrylonitrile:butadiene) and styrene butadiene rubber (SBR, 50:50 wt% of styrene:butadiene) matrices have been equilibrated by molecular dynamics (MD) simulations. Transition-state approach is used to calculate the diffusion and solubility coefficients of small penetrants in these matrices, indicating quite low values in NBR and reasonable agreement with experimental results. MD simulations have been performed to analyze water diffusion in these matrices. Aggregation of water molecules is observed in the hydrophobic matrix SBR. MD simulations with fictitious nonpolar water molecules inhibit aggregation and lead to enhanced diffusion in SBR. In NBR there is a slight increase in diffusion for fictitious water molecules. The lower diffusion constants in NBR result from slower local relaxation of the matrix due to tighter intermolecular packing and higher cohesive energy density. The free volume distribution that affects solubility coefficients is not a major determining factor for the diffusion coefficients in these matrices.

Keywords: Molecular dynamics simulation; Transition-state approach; Diffusion

1. Introduction

Poly(acrylonitrile-*stat*-butadiene), also called nitrile rubber (NBR), is a rubbery matrix having gas permeability close to glassy polystyrene. NBR is mainly utilized for products used in contact with hydrocarbon liquids, oils or greases. While glassy polymers usually show considerably lower constants of diffusion and sorption for small gas molecules than rubbery matrices, NBR being rubbery at room temperature, has lower permeability values compared to most of the glassy matrices. The reasons for the low permeability values of the rubbery NBR structure will be investigated in this study for the first time on a molecular basis.

Experimental and computational research on diffusion and sorption of small molecules in polymeric materials is essential due to the important applications of polymeric materials as membranes or barriers [1,2]. In order to understand the mechanisms of gas transport in the various polymers of interest, it is useful to relate the chemical composition of the polymer and its morphology to the sorption isotherms and diffusivities of penetrants within it. In this respect, molecular simulations have significant benefits in understanding the sorption and diffusion phenomena in polymers at the molecular scale [3].

Molecular dynamics (MD) simulations are valuable for the investigation of equilibrium and dynamic properties of polymeric microstructures at the molecular scale. MD has been extensively used in order to investigate the diffusion mechanism of small gas molecules in polymer matrices including poly(ethylene) [4,5], poly(propylene) [6,7], poly(isobutylene) [5,8–10], poly(dimethylsiloxane) [11–13], poly(butadiene) [14], poly(styrene) [15], poly(imide) and poly(amide imide) [16,17], poly(sulfones) [18,19], poly(benzoxazine) [20], poly(organophosphazenes) and poly(dibutoxyphosphazenes) [21,22], poly(ether-ether-ketone) [23], poly(styrene-*alt*-maleic anhydride) and poly(styrene-*stat*-butadiene) [24], poly(ethylene-*co*-vinyl alcohol) [25].

* Corresponding author. Tel.: +90 212 3597365; fax: +90 212 2575032.
E-mail addresses: doruker@boun.edu.tr, pemra@prc.boun.edu.tr (P. Doruker).

0032-3861/$ - see front matter © 2006 Elsevier Ltd. All rights reserved.
doi:10.1016/j.polymer.2006.08.062

Transition-state approach (TSA) [26,27] based on the transition-state theory is a computationally efficient, alternative method that is commonly used to predict the diffusion coefficients and the solubility values of small penetrants in polymer matrices. TSA is especially effective for polymeric systems with lower permeability coefficients, where MD simulations would not produce statistically reliable results due to computational time limitations [28–30].

The NBR structure used in this study consists of 61% butadiene and 39% acrylonitrile by weight. Our aim here is to understand the reasons underlying NBR's relative low permeability in comparison with another rubbery copolymer – styrene butadiene rubber (SBR: 50% butadiene and 50% styrene by weight). The glass transition temperatures of NBR (39%:61%) and SBR (50%:50%) matrices are −30 °C and −20 °C, respectively [31]. This specific SBR matrix has been investigated together with poly(styrene-*alt*-maleic anhydride) and polystyrene matrices in our previous work [24], where relatively short (2 ns) MD simulations have been utilized. In the current work longer simulations (6–10 ns) are performed, as a result of which aggregation of water molecules in the nonpolar SBR will be observed here for the first time.

First TSA will be utilized to determine the diffusion and solubility coefficients of small penetrants in the amorphous cells, which will give a clear indication of whether the cells have been adequately equilibrated. Next MD simulations of water diffusion in the equilibrated cells will be performed to study the aggregation of water molecules in SBR and the effects of hydrogen bonding on the diffusion constant in the polar matrix NBR. We will also assess the relative importance of chain packing, free volume distributions and local chain mobility in relationship with gas transport properties in these rubbery matrices.

2. Simulation details

Bulk structures of poly(styrene-*stat*-butadiene) and poly(acrylonitrile-*stat*-butadiene) were generated and simulated by using the commercial software of Accelrys (Insight II-Discover) [32] using the COMPASS (condensed-phase optimized molecular potentials for atomistic simulation studies) force field [33].

SBR chains contain styrene (50% by weight), and three types of butadiene repeat units (50% by weight in total): (i) *trans*-1,4, (ii) *cis*-1,4 and (iii) 1,2 or vinyl butadiene. The statistical copolymer chains of SBR are formed by using the reactivity ratios of 0.8 and 1.4 for styrene and butadiene, respectively [34]. Since each chain generated has a different random configuration (sequence), the weight percentages of different repeat units vary slightly among chains. The ratios of butadiene repeat units are adjusted according to the values given by Roff et al. [31], same as our previous study [24].

NBR chains also contain three types of butadiene repeat units (61% by weight in total): (i) *trans*-1,4, (ii) *cis*-1,4 and (iii) 1,2 or vinyl butadiene, and acrylonitrile (39% by weight). The copolymer chains of NBR are formed by using the reactivity ratios of 0.06 for acrylonitrile and 0.1 for butadiene [34]. The butadiene repeat units in NBR have similar ratios to those of SBR chains.

The degree of polymerization values, DP, and the total number of atoms, N_{atom}, including H atoms, for the constructed chains are given in Table 1.

2.1. Construction of amorphous cells

The generation of amorphous cells and their equilibration follows exactly the same procedure as described for SBR in our previous study [24]. The steps of this procedure can be summarized as follows: (i) formation of single chains of required length and composition, (ii) energy minimization of single chains, (iii) packing of isolated chains into periodic cells at reduced densities, (iv) NPT dynamics at 0.5 GPa and 300 K to bring the cells to the specified experimental densities, (v) energy minimization of cells, (vi) annealing of cells well above glass transition temperature, (vii) brief compression of cells (at 1 GPa for SBR and 0.5 GPa for NBR) followed by brief NVT dynamics both at 300 K, (viii) final equilibration by NPT dynamics at 1 bar and 300 K (more than 200 ps).

The average cell densities and the equilibrium cell lengths using the last 30 ps of the final NPT run are given in Table 1. As shown, densities obtained from dynamics, are very close to the experimental values.

In all runs, Andersen method was used for temperature control [35]. In NPT runs, the pressure was controlled by Berendsen's method, where 0.1 ps and 0.5 GPa^{-1} were used as the pressure scaling constant and system compressibility value, respectively [36]. During these simulations, the cutoff distance for the nonbonded interactions was taken as 12 Å both for SBR and NBR. The spline and buffer widths were 2 and 1.5 Å. The electrostatics were handled using atom-based approach. The time step was 1 fs in all simulation stages.

2.2. MD simulations of water diffusion in SBR and NBR

Diffusion of H_2O molecules in the equilibrated cells of SBR-1, SBR-3 and NBR-1 were monitored by NVT dynamics at 300 K. For this aim, five H_2O molecules were inserted into the equilibrated SBR and NBR microstructures. The water content corresponds to 1% by weight in all these structures.

Table 1
Details of the simulation systems

System	DP	N_{atom}	ρ_{exp} (g/cm^3)	ρ_{sim}[a] (g/cm^3)	Error[b] (%)	Cell lengths[c] (Å)
SBR-1	120	1448	0.98	0.970	1.0	24.46
SBR-2	120	1448	0.98	0.950	3.1	24.65
SBR-3	120	1448	0.98	0.960	2.0	24.54
NBR-1	164	1450	1.00	0.974	2.6	24.67
NBR-2	164	1450	1.00	0.962	3.8	24.78
NBR-3	164	1450	1.00	0.963	3.7	24.76

[a] Equilibrium density of each system is calculated as an average over the final 30 ps of the equilibration NPT runs. Standard deviation is in the range of 0.006–0.009 during this period.
[b] Error(%) = $|(\rho_{exp} - \rho_{sim})| \times 100/(\rho_{exp})$.
[c] Calculated as an average over the final 30 ps of the equilibration NPT runs.

The water molecules were positioned at the free volume sites of the cells such that the distance between any pair of H_2O was at least 10 Å. After insertion of water molecules, the systems were subjected to energy minimization first by fixing the polymer atoms and afterwards by setting them again free.

In these calculations, the velocity Verlet algorithm was used with a time step of 1 fs. The cutoff distance for nonbonded interactions was set to 11 Å, using respective spline and buffer widths of 2 and 1.5 Å.

The diffusion coefficients, D, of the water molecules can be calculated by means of the Einstein relation.

$$D = \frac{\langle r^2 \rangle}{6t}, \quad t \to \infty \tag{1}$$

here $\langle r^2 \rangle = \langle |\boldsymbol{r}(t) - \boldsymbol{r}(0)|^2 \rangle$ is the mean square displacement (MSD) of the penetrants over time, t. The brackets show that the average was taken for all the penetrant molecules over all time origins.

2.3. TSA

TSA is used to compute the solubility values (S) and diffusion coefficients (D) for various kinds of gases in the generated amorphous polymer microstructures [26–28]. The COMPASS force field and the programs gsdif and gsnet are used for all TSA calculations [37]. The methodology used here is the same as in our previous study [24].

TSA assumes that gases diffuse through dense polymer systems by a series of activated hops, which are independent from the structural relaxation of the polymer matrix and depend only on the elastic motion of the matrix [28]. This assumption is only valid for the diffusion of small molecules (not larger than methane) through the polymers. The isotropic elastic motion of the matrix is characterized by a smearing factor, which represents the fluctuations (MSD) of the polymer atoms around their equilibrium positions. A smearing factor, which is taken as identical for all the atoms in the matrix, is calculated for each gas using the self-consistent field procedure option of gsnet [37].

An equilibrated amorphous cell is transformed into an orthogonal lattice with a constant spacing of 0.3 Å. The solute distribution function in the matrix, $\rho(\boldsymbol{r})$, is evaluated by calculating the interaction energy between a gas molecule inserted at each grid point and all the atoms of the polymer matrix that are subjected to elastic fluctuations. As a result, the local maxima in $\rho(\boldsymbol{r})$ are identified as different free volume sites in the matrix. The rate constants and the probabilities for the penetrant jumps from one free volume site to another are then determined together with the residence times in each site.

Once the smearing factor and the corresponding jump probabilities are determined, the trajectories of the penetrant molecules are calculated by a Monte Carlo (MC) type procedure. The diffusion coefficient, D, is then obtained as an average over 1000 independent MC trajectories.

For low pressures ($p \ll 1$), the solubility, S, can be computed by using the TSA [28],

$$S = \frac{1}{kTV} \int \rho(\boldsymbol{r}) \mathrm{d}V \tag{2}$$

here k represents the Boltzmann's constant and T is the temperature. The integral over the volume of the amorphous cell is actually a summation over all the lattice sites.

Once the diffusion and solubility values are computed, the permeability, P, values can be calculated by the relation $P = DS$.

3. Results and discussion

3.1. Evaluation of constructed amorphous cell structures by TSA

Our first step is to determine the diffusion and solubility values of small gases in three equilibrated amorphous cells of NBR (NBR-1, NBR-2 and NBR-3) by using TSA and compare these values with the experimental results in literature. Provided that these physical properties are satisfactory, we will further assess the molecular dynamics simulations performed with these cells. The TSA results for the other rubbery matrix SBR, which has a much higher permeability, are also provided here for comparison. In this section, the averages for SBR are taken over the same two SBR structures (SBR-1 and SBR-2) from our previous study [24], plus another independent cell, SBR-3. The reason for using three independent structures instead of two is to better observe the effect of different random copolymer sequences on the physical properties of NBR and SBR.

Table 2 gives the computed densities, free volume percentages and solubility parameters, $\delta_{(\mathrm{sim})}$, of the specific snapshots chosen for the TSA calculations. The free volume calculations were done by the TSA of Gusev and Suter [26–28]. The free volume percentage is the ratio of the total free volume of the cell (V_f) to the total volume of the amorphous cell. The solubility parameters ($\delta = (\Delta E/V)^{1/2}$ where ΔE is the cohesive energy and V is the molar volume) computed for NBR and SBR are slightly underestimated. The errors vary between 10 and 11% for SBR, and between 12 and 13% for NBR. The higher solubility parameter of NBR compared to SBR arises from the favorable interactions of polar acrylonitrile groups belonging

Table 2
Properties of the specific cells chosen for TSA calculations

System	ρ[a] (g/cm^3)	Free volume[d] (%)	Solubility parameters	
			$\delta_{(\mathrm{exp})}$ (MPa)$^{1/2}$	$\delta_{(\mathrm{sim})}$[e] (MPa)$^{1/2}$
SBR-1	0.974	4.9		14.9
SBR-2	0.957	7.2	17.5–17.8[b]	15.9
SBR-3	0.960	7.0		16.9
NBR-1	0.985	4.2		19.3
NBR-2	0.976	4.8	21.1–21.4[c]	17.6
NBR-3	0.970	4.6		19.1

[a] Density of the specific cell used for TSA.
[b] Experimental data for butadiene/styrene 60:40 (wt:wt parts %) [34].
[c] Experimental data for butadiene/acrylonitrile 61:39 (wt:wt parts %) [34].
[d] Free volume % = (V_f/total volume of the amorphous cell) × 100.
[e] $\delta_{(\mathrm{sim})} = (\Delta E/V)^{1/2}$.

to different chains. The higher solubility parameter and the relatively smaller side groups of NBR lead to a reduced fractional free volume.

Averages of the diffusion and solubility values of small penetrant molecules in these structures computed by TSA are plotted according to the correlations of Teplyakov and Meares [38].

$$\log D = K_1 - K_2 d_{\text{eff}}^2 \tag{3}$$

$$\log S = K_3 + K_4(\varepsilon/k) \tag{4}$$

The correlation of D with the effective penetrant diameter (d_{eff}) is illustrated in Fig. 1, whereas the correlation of S with the Lennard–Jones potential well-depth (ε/k) is shown in Fig. 2. The correlation coefficients K_1–K_4 depend on the chemical and physical properties of the polymer matrices [38].

The filled circles in Fig. 1 represent the D_{exp} values of NBR [34,39]. The factor $D_{\text{sim}}/D_{\text{exp}}$ is in the range of 1.3–2.0 except for the smaller gases He ($D_{\text{sim}}/D_{\text{exp}} = 2.5$) and H_2 ($D_{\text{sim}}/D_{\text{exp}} = 2.8$). Diffusion coefficient estimates by TSA seem to be in fairly good agreement with the experimental values. D_{exp} values for SBR [31] are provided for 23% styrene content by weight rather than the 50% styrene content used in our simulations, indicating reasonable agreement between computations and experiments. A more detailed comparison with other experiments has been provided for SBR [24]. Furthermore, the contribution of the new SBR-3 to the average of the two cells used in our previous study [24] resulted in a slight decrease of the average diffusion coefficients especially for the larger gases. This indicates the importance of averaging over several independent cells for property estimation, which corresponds to different local minima of the conformational energy surface. Averaging may be even more crucial in the case of random copolymers with bulky side groups, where each amorphous cell contains a single chain with a different sequence.

The filled circles in Fig. 2 represent the S_{exp} values of NBR. The computed solubility coefficients (empty circles)

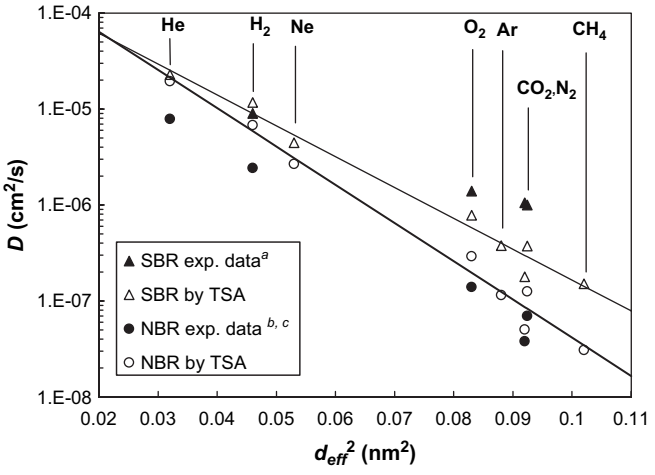

Fig. 1. Diffusion coefficients computed by TSA as a function of (d_{eff}^2) for SBR (50% styrene by weight) and NBR (39% acrylonitrile) systems. Experimental data are provided for NBR (39% acrylonitrile) [34,39] and SBR (23% styrene) [31].

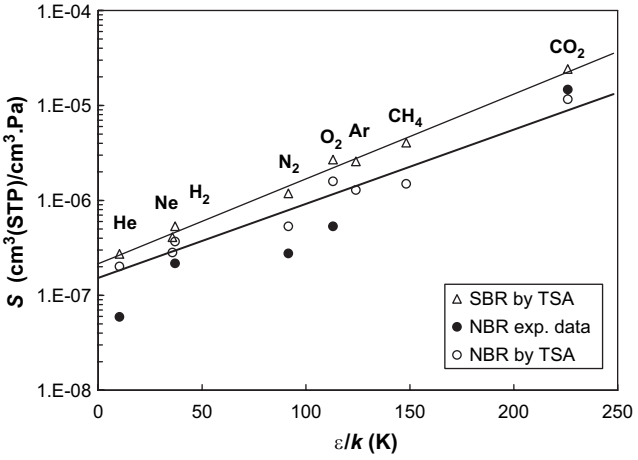

Fig. 2. Solubility values computed by TSA, as a function of the penetrant Lennard–Jones potential well-depth (ε/k) for SBR and NBR. Experimental data [34] are provided for NBR (39% acrylonitrile).

are generally higher than the experimental values. The factor $S_{\text{sim}}/S_{\text{exp}}$ changes between 1.7 and 3.4 with the exception of CO_2 ($S_{\text{sim}}/S_{\text{exp}}$ is 0.79 for CO_2) in NBR. Similar differences between experimental and computed solubility values have also been observed in previous TSA studies [28,29].

The lines in Figs. 1 and 2 are drawn through the TSA results according to Eqs. (3) and (4) and represent the least squares fit through average D_{sim} and S_{sim} values for each matrix with R^2 values of 0.98 in all cases.

In general, the TSA results shown in Figs. 1 and 2 seem to be in reasonable agreement with the experimental values, i.e., there is less than one order of magnitude difference. Therefore, it can be concluded that the amorphous cells represent realistic bulk structures. Even though the SBR and NBR structures are both rubbery, their gas transport properties differ considerably. Both the diffusion and the solubility coefficients of NBR are smaller than SBR and the differences between the diffusion coefficients of the two structures increase as the effective penetrant diameter increases.

Up to this point, gas transport coefficients for the final equilibrated SBR and NBR cells in Table 2 have been identified. Since these matrices are rubbery, there is considerable relaxation of the chains compared to the frozen glassy matrices during MD simulations. It is known that the size and shape of the free volume sites in rubbery polymers change considerably with time [13]. Therefore, variations should be observed in the free volume distributions, and possibly in gas transport properties calculated by TSA, if different snapshots are taken during the course of NPT dynamics after equilibration. In contrast, the CED of a cell does not vary significantly during a specific MD run, since its value is initially determined by the amorphous packing of the single chain. In what follows next, four to six snapshots are taken from the last 50,000 fs of the final NPT (at 1 bar and 300 K) dynamics of each amorphous cell. The cells are characterized in terms of their total free volume percentages and gas transport coefficients by TSA.

The diffusion and solubility coefficients of O_2 gas calculated by TSA are plotted as a function of the total free volume

percentage of specific snapshots in Fig. 3(a) and (b), respectively. In Fig. 3(a) the scattering of D_{sim} values for SBR snapshots is much more pronounced compared to NBR cells. A significant correlation is not observed among the diffusion coefficients and the total free volume percentages of the individual snapshots. However, looking at the average D_{sim} values for SBR ($64 \pm 40 \times 10^{-8}$ cm^2/s) and NBR ($22 \pm 13 \times 10^{-8}$ cm^2/s) snapshots indicates that NBR having smaller free volume content has also a smaller average D_{sim} for O_2. Thus, we cannot rule out the free volume of rubbery matrices as a factor affecting the diffusion coefficients, especially when the size of the gas molecule is considerably large.

Fig. 3(b) indicates a high correlation (linear correlation coefficient $R^2 = 0.82$) between the total free volumes and the solubility coefficients of the individual snapshots. As the total free volume content of the amorphous cell structure increases, the solubility coefficient also increases, consistent with the results of our previous work [24]. Interestingly, the free volume distributions of the SBR-1 snapshots are very similar to the NBR structure and therefore their solubility coefficients fall within the same range as NBR snapshots. In general, the bulky side groups of the SBR chain may be the reason for the high variations that are observed in the gas transport coefficient and the free volume distributions of its different snapshots.

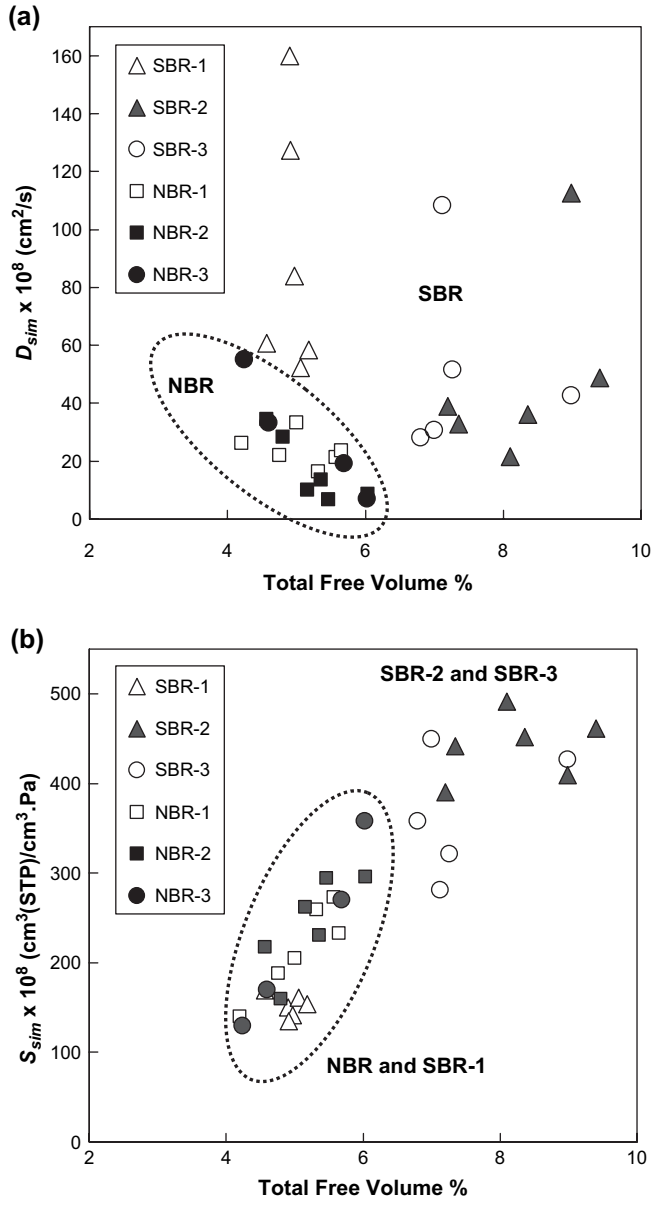

Fig. 3. Computed (a) D_{sim} and (b) S_{sim} values of O_2 as a function of the total free volume percentages for the individual snapshots of SBR and NBR microstructures (TSA results).

3.2. Diffusion of water molecules from MD simulations

The diffusion of water molecules is investigated in the amorphous cell structures of NBR-1, SBR-1 and SBR-3. Specifically, SBR-1 has a lower total free volume content compared to SBR-3, but on the other hand SBR-3 has a higher CED (see Table 2). In comparison, the properties of the different NBR cells generated are quite uniform and therefore only one NBR cell will be focused on.

The effect of hydrogen bonding (H-bonding) on water diffusion through hydrophobic (SBR) and hydrophilic (NBR) amorphous structures is investigated by considering polar and nonpolar (fictitious) water molecules. The effect of water aggregation on the free volume distributions of these matrices will be reported as a result of prolonged simulations (the simulation time is 10 ns for SBR-1 and 6 ns for all other structures).

3.2.1. Mobility of water molecules

The displacement of each water molecule from its initial position, $\boldsymbol{r}(t) = \sqrt{|\boldsymbol{r}(t) - \boldsymbol{r}(0)|^2}$ to its position at time t is displayed in Fig. 4 for SBR and NBR. Fig. 4(a) shows the change in $\boldsymbol{r}(t)$ as a function of time for SBR-1, three representative water molecules are chosen and the curves for H_2O-1 and H_2O-2 molecules have been shifted vertically by 25 and 14 Å for better visualization. Within the first 3 ns, considerable displacement of the molecules takes place. The diffusion of water molecules in SBR-1 matrix during the first 2 ns of this simulation has already been reported in comparison with polystyrene and styrene-maleic anhydride copolymer [24]. At the end of 3 ns, all water molecules aggregate and form a cluster in this nonpolar SBR matrix. From this point on, the molecules do not make any significant jumps, but instead wobble back and forth within the same region of free volume. Similar behavior is observed in SBR-3 (not shown), where four out of five water molecules form a cluster that is stable during 3–6 ns.

Fig. 4(b) shows the displacement of water molecules in NBR-1 cell during 6 ns. Two representative water molecules are chosen in this case and the curve for H_2O-1 is shifted vertically by 4 Å. The water molecules do not form clusters in the NBR cell, nevertheless their displacements are considerably lower.

One of the reasons for the less frequent jumps in NBR could be the H-bonding occurring between the acrylonitrile groups of NBR and the water molecules. On the other hand, the clustering of water molecules within the SBR structure occurs due to the H-bonding among different water molecules.

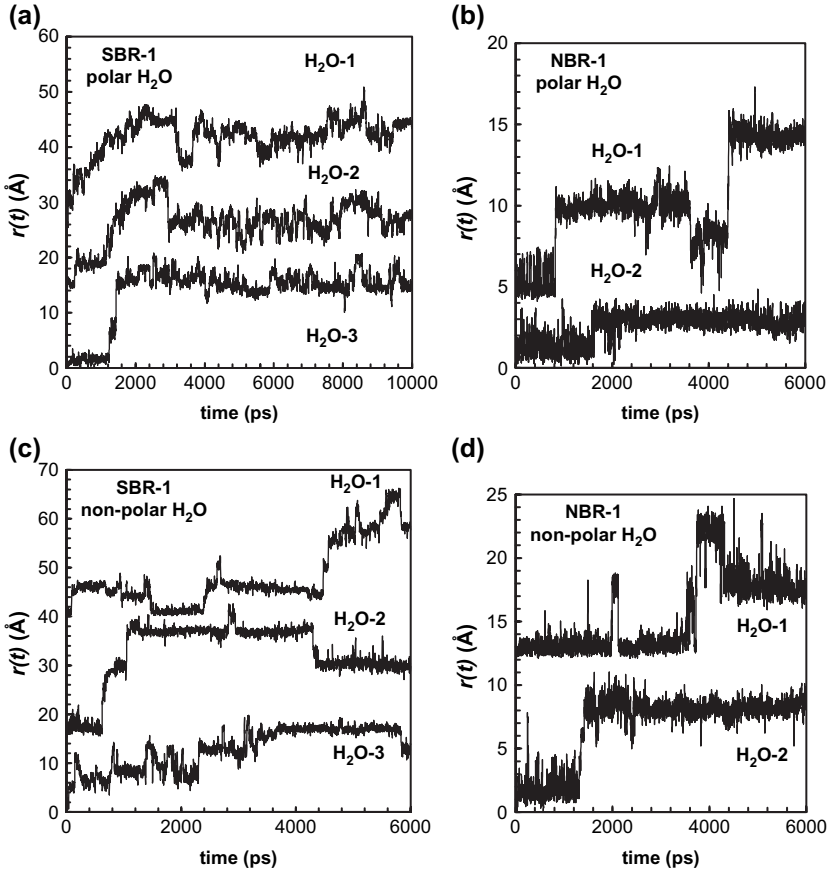

Fig. 4. Displacements of: (a) polar H_2O in SBR-1; (b) polar H_2O in NBR-1; (c) nonpolar H_2O in SBR-1 ($q = 0$); (d) nonpolar H_2O in NBR-1 ($q = 0$).

In general terms, H-bonding stems from the electrostatic interactions resulting from the partial charges assigned to atoms, i.e., the oxygen and hydrogen atoms of water molecules, and the nitrogen atom of acrylonitrile groups. To quantify the effect of H-bonding on diffusivity, NVT simulations are also performed by eliminating the partial charges on water molecules ($q = 0$), i.e., treating water as a fictitious, nonpolar molecule of the same size. As a result, the electrostatic interactions between water molecules and the NBR chain and the clustering of water molecules in SBR are avoided. Thus, only the effects of chain mobility, free volume distributions and chain packing remain for consideration.

The displacement of the three representative nonpolar water molecules in SBR-1 is shown in Fig. 4(c) for 6 ns. The curves for H_2O-1 and H_2O-2 molecules (shifted vertically by 40 and 15 Å) indicate continuous jumps, due to inhibition of clustering. On the other hand, no significant difference is observed for the case of NBR (Fig. 4(d)). This shows that the hydrogen bonding between the water molecules and the polymer chain of NBR is not the main reason for the less frequent jumps occurring in NBR.

3.2.2. Water diffusion through amorphous cells

Fig. 5(a) shows the MSD of water molecules as a function of time in NBR-1 and SBR-1 structures during 6 ns. The initial MSD of water in SBR-1 (curve 2) is faster than in NBR-1 (curve 4). After 2.5 ns, the MSD slows down in SBR-1, due to the clustering of water molecules. The thin dashed lines in Fig. 5(a) have a slope of one and they represent the transition from the nonEinstein (anomalous) diffusion regime to the Einstein diffusion regime. Due to the aggregation of water molecules in the SBR structure, it is not possible to observe the Einstein diffusion regime within the time frame of 0–6 ns for curve 2. On the other hand, the Einstein diffusion regime is observed after 3 ns for NBR. The MSD curves for the nonpolar water molecules are represented by number ''1'' for SBR and number ''3'' for NBR. Both of these curves reached the Einstein diffusion regime almost at the same time (2.5 ns).

The D_{sim} values estimated for specific runs are reported in Table 3. When there is clustering of water molecules (SBR-1 and SBR-3), the Einstein diffusion regime is not observed for the case of longer simulation times (above 3 ns), hindering the diffusion coefficient estimations. The MSD curves for nonpolar (fictitious) and polar (realistic) water molecules are averaged over SBR-1 and SBR-3 cells in Fig. 5(b), which indicates clearly the clustering of water molecules inside the SBR structures. When clustering of water molecules is removed, D_{sim} values of SBR are nearly one order of magnitude higher than the D_{sim} values of NBR. However, it should be noted that three-dimensional diffusion is not exactly observed if the motion of individual water molecules is tracked during 6 ns. In most cases, one of the principal moments of the radius of gyration tensor is considerably greater than the other two. Thus, the diffusion coefficients reported should be taken

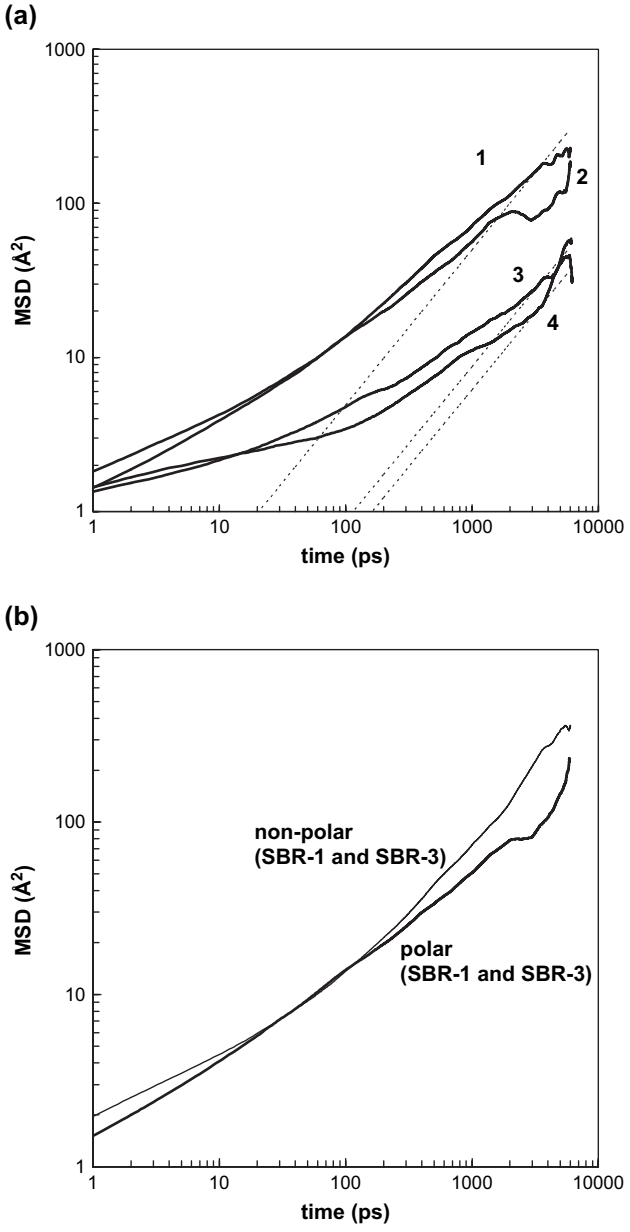

Fig. 5. Logarithmic plots of MSD vs. time: (a) water diffusion in SBR-1 (curves 1 and 2) and NBR-1 (curves 3 and 4). Curves 1 and 3 represent the diffusion of fictitious, nonpolar water molecules; (b) averages of SBR-1 and SBR-3 with polar and nonpolar H_2O molecules.

Table 3
Diffusion coefficients, D_{sim}, of water in SBR and NBR from MD simulations

System	Water type	Time range (ns)	$D_{sim} \times 10^8$ (cm^2/s)
SBR-1	Polar (curve 2)[a]	0–10	–
	Nonpolar (curve 1)	0–6	79
SBR-3	Polar[a]	0–6	–
	Nonpolar	0–6	146
NBR-1	Polar (curve 4)	0–6	10
	Nonpolar (curve 3)	0–6	14

[a] Diffusion coefficients could not be calculated due to the aggregation of water molecules.

with caution, since they do not represent random walk of individual penetrants in three-dimensions, which could be improved by longer simulations.

There are no experimental data for the water diffusion coefficients in SBR and NBR. The D_{sim} value of water in NBR is found to be within the same range of O_2, in accordance with the simulation results on polybenzoxazine [20].

3.3. Pair correlation functions

To obtain further insights about chain packing, the pair correlation function, $g(r)$, is calculated for SBR-1, SBR-3 and NBR-1 systems. Fig. 6(a) and (b) shows the intermolecular and total pair correlation functions for the main chain atoms, respectively. Here in the case of a single chain considered, the intermolecular $g(r)$ refers to the interactions of the carbon atoms of the main chain with carbon atoms on the periodic images of itself, while the total $g(r)$ is the summation of the intermolecular $g(r)$ and intramolecular $g(r)$. Intramolecular $g(r)$ includes the interactions between all pairs of carbon atoms on the single main chain in unperturbed (unpacked) conditions.

The $g(r)$ is averaged over 6000 snapshots between 0 and 6 ns. The calculations performed for runs with nonpolar and polar water do not indicate any significant difference. The intermolecular $g(r)$ shows a peak around 5.35 Å for all systems. The magnitude of $g(r)$ at this peak in Fig. 6(a) increases in the following order: SBR-1 < SBR-3 < NBR-1, which is the same as the order of the CED values of these matrices.

The total $g(r)$ curves of SBR-1 and SBR-3 are similar (not shown), so the total $g(r)$ shown in Fig. 6(b) for SBR is the average of the two structures. The peaks in total $g(r)$ at $r < 4$ Å result from the bonded interactions. In total $g(r)$, there is a slight difference between NBR and SBR in the region of 5–8 Å. Furthermore, in Fig. 6(c) $g(r)$ for side chains of NBR-1 (nitrogen atoms) and SBR-1 (carbon atoms on the phenyl ring) is compared. Here, it is also seen that the side chains are more closely packed in NBR. A larger value of $g(r)$ indicates that the number of nearest neighbors within a distance r from a central atom is bigger.

In summary, Fig. 6 indicates that the molecular packing of the polymer chain is tighter in NBR than in SBR-1 and SBR-3, a fact that is related to the higher cohesive energy density in NBR and that may at the same time contribute to the lower diffusivity in NBR.

Fig. 7 exhibits the interactions between the atoms of H_2O molecules and some selected atoms of polymer chains. In Fig. 7(a), $g(r)$ between the nitrogen atoms (n1t) of the NBR chain and the hydrogen atoms (h1o) of water shows a sharp peak at a distance of ≈1.95 Å, which indicates the occurrence of H-bonding. In the same figure, the thin line indicates $g(r)$ for the uncharged hydrogens of water molecules and nitrogens of NBR, where H-bonding does not exist.

The interactions between different water molecules (in this case the interaction site for the water molecule is chosen as the oxygen atom) residing in the same SBR-1 cell are displayed in Fig. 7(b) averaged over three different simulation time ranges: 0–2, 0–6 and 0–10 ns. The high peaks located at about

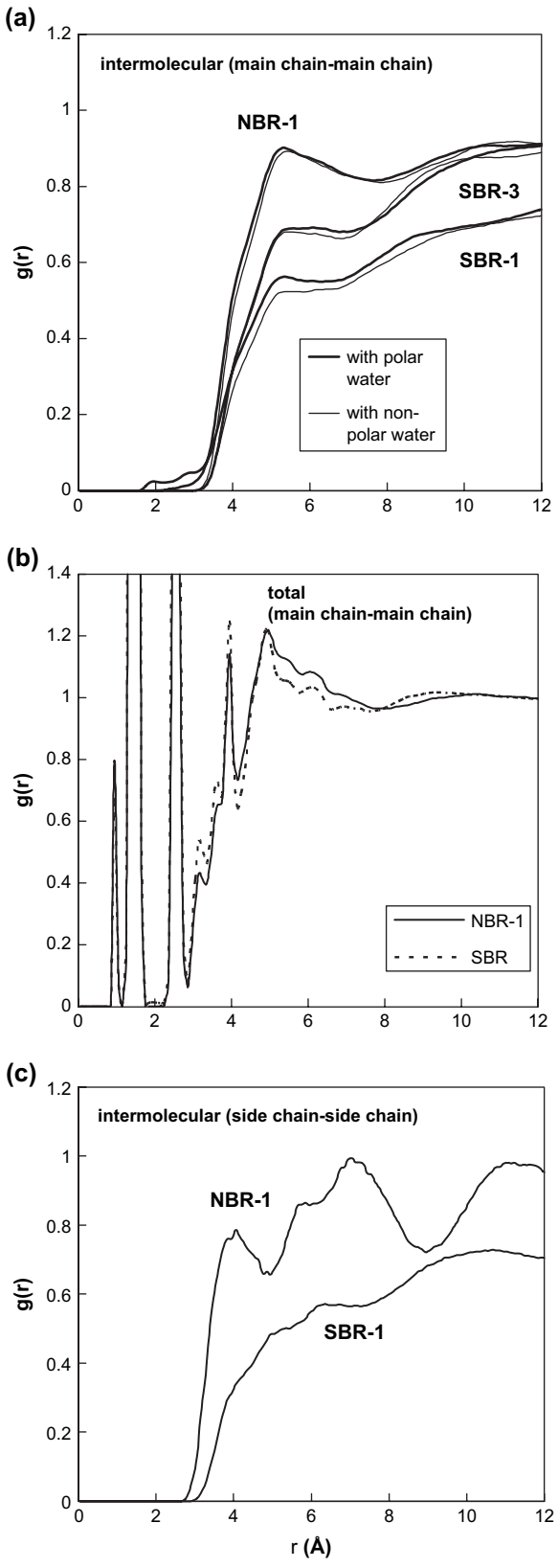

Fig. 6. Pair correlation functions: (a) chain–chain intermolecular $g(r)$ for NBR-1, SBR-3 and SBR-1; (b) total $g(r)$ for NBR and SBR; (c) intermolecular $g(r)$ for side chains of NBR and SBR.

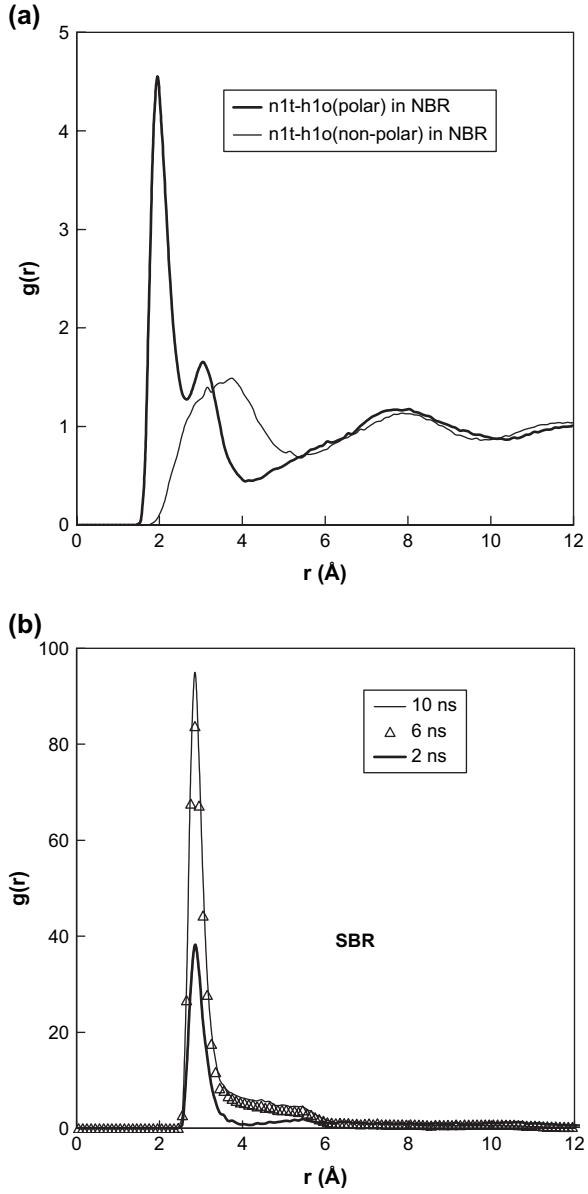

Fig. 7. Intermolecular $g(r)$ for: (a) hydrogen (h1o) atoms of water molecules with nitrogen (n1t) atoms of NBR; (b) oxygen atoms of polar water molecules among themselves in SBR cell.

2.85 Å indicate that there is appreciable self-aggregation among water molecules in the nonpolar system of SBR, which becomes more pronounced as a function of time. The effect of the aggregation of water molecules on the accessible free volume fractions of SBR will be discussed next.

3.4. Dynamics of free volume distributions

The dynamics of the free volume distributions during NVT simulations are also investigated for SBR-1 and NBR-1 matrices using TSA with He gas as the probe molecule [26–28]. The same procedure used in our previous study is followed for the estimation of total free volume and the free volume fraction, f_a [24]. Here f_a gives the free volume fraction of the cavities that have sizes equal or greater than a threshold

cavity volume, thus f_a decreases as the threshold volume increases. The long-standing clusters of water molecules in the SBR-1 matrix might affect the free volume distribution of the whole cell. So the free volume distributions of the matrices along the trajectory are computed. The free volume distributions are determined after removing all water molecules inside the cell. This actually reveals the sizes of cavities (site free volume, $Å^3$) that the water molecules reside in.

The volume fractions of cavities (f_a) are computed for the SBR-1 and NBR-1 structures at every 1 ns of NVT-MD dynamics run with polar water and nonpolar water molecules. In Fig. 8(a), the filled and empty squares represent f_a as a function of threshold cavity size for the NBR cells with nonpolar and polar water molecules, respectively. The snapshots at the end of each nanosecond from the 6 ns NVT trajectories are chosen. Since the free volume distributions of the cells do not show a dependence on time, the time frame that they represent is not indicated on the curves and only the snapshot at 4 ns with polar water molecules shows a distinct behavior from the rest. At that point, two large free volume sites are detected in the cell structure, which do not exist in the other snapshots analyzed. The cavities, that the nonpolar water molecules reside in, seem to be larger compared to the polar water molecules, which is a result of the intermolecular electrostatic interactions being turned off.

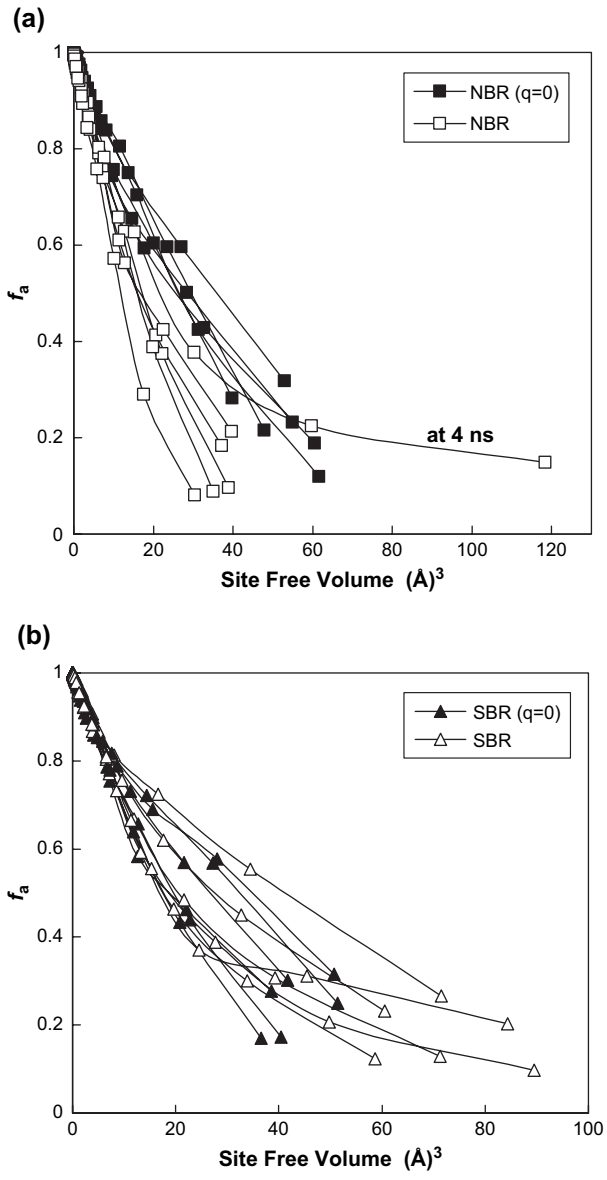

Fig. 8. Dynamics of free volume distributions, showing the volume fractions of cavities, f_a, as a function of threshold cavity size throughout the MD simulations performed for: (a) NBR-1; (b) SBR-1. Snapshots at the end of 1 ns interval are shown. Fictitious, nonpolar water molecules are indicated by $q = 0$.

The filled triangles in Fig. 8(b) represent f_a for SBR-1 at the end of 1, 2, 3, 4, 5 and 6 ns for nonpolar water molecules. The empty triangles represent f_a for the snapshots from polar water simulations after clustering, which are chosen at the end of 5, 6, 7, 8, 9 and 10 ns. As already discussed, the polar water molecules form a long-standing cluster inside the SBR-1 structure, which results in the lengthening of the curves to larger volumes.

The average total free volume percentages of the displayed NBR-1 snapshots are 7.0 ± 0.6 (nonpolar water) and 5.3 ± 0.6 (polar water). Similarly, those for SBR-1 snapshots are 6.4 ± 0.5 (nonpolar water) and 6.5 ± 0.6 (polar water). Even though the average total free volume of NBR-1 with nonpolar water molecules is similar to that of SBR-1, the diffusion in NBR cell is much slower. This result suggests that the free volume content is not the major determining factor on the small gas diffusion mechanism in these matrices. In a recent study with semi-flexible model polymer chains, chain flexibility has been found to be more influential on diffusion than free volume distributions [43]. Next we will assess the local chain mobility of the two matrices, which is closely tied up with chain flexibility.

3.5. Local mobility of polymer chains

As also shown in our previous studies [24,25], the diffusion of small penetrants in polymers is correlated with the relaxation of polymer chains. Till now it is observed that the diffusion of small penetrant molecules (including water molecules) in NBR is appreciably slower compared to that in SBR. Therefore, the local dynamics of the two matrices are compared here using the rotational (orientational) time correlation function [40,41].

$$m(t) = \langle \boldsymbol{u}(t_0) \cdot \boldsymbol{u}(t_0 + t) \rangle \tag{5}$$

where the unit vector $\boldsymbol{u}(t)$ connects any C(i) and C($i+1$) along the main chain. The ensemble average is evaluated on the basis of an ensemble of snapshots at various starting times, t_0.

Fig. 9 shows the rotational time correlation functions for the main chain vectors of SBR-1, SBR-3 and NBR-1 over the 6 ns dynamics in the presence of water molecules. The curves do not level off to a constant value as in the case of glassy polymers, but they do show a continual decay. The slower relaxation of the NBR chain compared to SBR is one of the main reasons for the slower gas diffusion observed in it. SBR-1 and SBR-3 show similar relaxation behavior, as

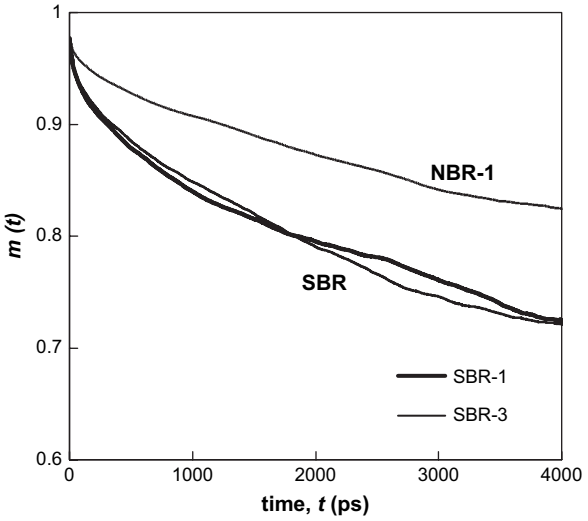

Fig. 9. The rotational time correlation function during NVT dynamics for the main chain vectors of SBR and NBR, exhibiting local mobility of the chains.

expected. The relaxation times, τ, are also obtained by fitting $m(t)$ to the empirical Williams–Watts expression;

$$m(t) = A \exp\left[-(t/\tau)^{\beta} \right] \tag{6}$$

where $\beta = 1$ [42]. The fitting is performed for the time range of 0–1 ns. τ values for SBR and NBR are found to be 8.3 and 16.4 ns, respectively.

In fact, the bulky side groups (e.g. the styrene of SBR chain) or more rigid backbone groups in a polymer usually restrain the local chain mobility and this mainly increases its glass transition temperature. On the other hand, in a polymer chain having polar groups and a higher CED, the chain mobility is suppressed due to tighter chain packing (e.g. NBR structure). Comparison of the diffusion coefficients in SBR (50 wt% butadiene) and NBR (61 wt% butadiene) indicates that CED is more effective in terms of suppressing local mobility for this case.

4. Concluding remarks

NBR, being a rubbery copolymer, has gas permeability values that are on the order of glassy matrices such as polystyrene and much lower than other rubbery matrices. Our aim in this study is to characterize the equilibrium and dynamic properties of NBR at the molecular scale, in comparison to another nonpolar rubbery matrix of SBR. In conformity with experiments, our TSA and MD simulation results indicate that small gas diffusion in the polar matrix of NBR is significantly lower compared to SBR. Based on TSA results, independent equilibrated cells of NBR exhibit more uniform properties in terms of diffusion, solubility coefficient and free volume distribution in comparison to the more scattered behavior of SBR cells that may result from the bulky styrene side groups.

The water molecules form hydrogen bonding with the polar groups of NBR. However, these hydrogen bonds, if eliminated by using nonpolar water molecules, do not seem to affect the diffusion significantly. In contrast, in the nonpolar SBR, there is clustering of the water molecules, which results in a lowering of diffusion with time and an increase in cavity size. When nonpolar water molecules are used, aggregation of water molecules is prohibited and as a result of which diffusion increases appreciably.

The free volume distributions of the matrices correlate closely with the solubility coefficients, but not with the diffusion constants. In fact, the orientational autocorrelation function of the backbone bonds show faster chain relaxation in SBR compared to NBR, which seems to be the major determining factor for the higher diffusion in SBR. Even though the bulky side groups in SBR chain restrain the local chain mobility, it is observed that the tighter intermolecular packing (higher CED due to the presence of polar side groups) is more dominant in the suppression of chain relaxation and gas diffusion in NBR compared to SBR.

Acknowledgment

This work has been supported by the Bogazici University B.A.P. (Projects 03A501-D and 04S106), TUBITAK Project 104M247, DPT Project (03K120250), and the Turkish Academy of Sciences in the framework of the Young Scientist Award Program (PD-TUBA-GEBIP/2002-1-9).

References

[1] Comyn J. Polymer permeability. 2nd ed. Great Britain: Chapman & Hall; 1994.
[2] Vieth WR. Diffusion in and through polymers. Munich; Vienna; New York; Barcelona: Hanser; 1991.
[3] Theodorou DN. In: Neogi P, editor. Diffusion in polymers. New York: Marcel Dekker Inc.; 1996. p. 67.
[4] Müller-Plathe F. J Chem Phys 1991;94:3192.
[5] Pant PVK, Boyd RH. Macromolecules 1993;26:679.
[6] Cuthbert TR, Wagner NJ, Paulaitis ME, Murgia G, D'Aguanno B. Macromolecules 1999;32:5017.
[7] Müller-Plathe F. J Chem Phys 1992;96:3200.
[8] Boyd RH, Pant PVK. Macromolecules 1991;24:6325.
[9] Müller-Plathe F, Rogers SC, van Gunsteren WF. Macromolecules 1992;25:6722.
[10] Müller-Plathe F, Rogers SC, van Gunsteren WF. J Chem Phys 1993;98:9895.
[11] Tamai Y, Tanaka H, Nakanishi K. Macromolecules 1994;27:4498.
[12] Sok RM, Berendsen HJC, van Gunsteren WF. J Chem Phys 1992;96:4699.
[13] Charati SG, Stern SA. Macromolecules 1998;31:5529.
[14] Gee RH, Boyd RH. Polymer 1995;36:1435.
[15] Han J, Boyd RH. Polymer 1996;37:1797.
[16] Hofman D, Ulbrich J, Fritsch D, Paul D. Polymer 1996;37:4773.
[17] Zhang R, Mattice WL. J Membr Sci 1995;108:15.
[18] Niemela S, Leppanen J, Sundhol F. Polymer 1996;37:4155.
[19] Wang X, Veld PJ, Lu Y, Freeman BD, Sanchez IC. Polymer 2005;46:9155.
[20] Kim WK, Mattice WL. Macromolecules 1998;31:9337.
[21] Fried JR, Ren P. Comput Theor Polym Sci 2000;10:447.
[22] Hu N, Fried JR. Polymer 2005;46:4330.
[23] Tocci E, Hofman D, Paul D, Russo N, Drioli E. Polymer 2001;42:521.
[24] Kucukpinar E, Doruker P. Polymer 2003;44:3607.
[25] Kucukpinar E, Doruker P. Polymer 2004;45:3555.

[26] Gusev AA, Arizzi S, Suter UW, Moll DJ. J Chem Phys 1993;99:2221.
[27] Gusev AA, Suter UW. J Chem Phys 1993;99:2228.
[28] Gusev AA, Müller-Plathe F, van Gunsteren WF, Suter UW. Adv Polym Sci 1994;116:207.
[29] Hofman D, Fritz L, Ulbrich J, Paul D. Comput Theor Polym Sci 2000; 10:419.
[30] Lopez-Gonzales M, Saiz E, Guzman J, Riande E. J Chem Phys 2001; 115:6728.
[31] Roff WJ, Scott JR, Pacitti J. Fibres, films, plastics and rubbers: a handbook of common polymers. 1st ed. London: Butterworths; 1971.
[32] Accelrys Inc. Insight II 4.0.0 P+, POLYMERIZER, DISCOVER, AMORPHOUS_CELL, BUILDER and RIS Modules version 2001.11. San Diego, CA, USA; 2001.
[33] COMPASS – condensed phase optimized molecular potentials for atomistic simulation studies; 1999. Distributed by Accelrys Inc.
[34] Brandrup J, Immergut EH, Grulke EA. Polymer handbook. 4th ed. Canada: John Wiley & Sons Inc.; 1999.
[35] Andersen HC. J Chem Phys 1980;72:2384.
[36] Berendsen HJC, Postma JPM, van Gunsteren WF, DiNola A, Haak JR. J Chem Phys 1984;81:3684.
[37] GSNET & GSDIF Macros. Distributed by Accelrys Inc., San Diego, CA, USA; 2001.
[38] Teplyakov V, Meares P. Gas Sep Purif 1990;4:66.
[39] Van Krevelen DW. Properties of polymers. Netherlands: Elsevier Science Publishers; 1990 [chapter 18].
[40] Allen MP, Tildesley DJ. Computer simulation of liquids. Oxford: Clarendon Press; 1989.
[41] Bahar I, Badur B, Doruker P. J Chem Phys 1993;99:2235.
[42] Tamai Y, Tanaka H. Fluid Phase Equilib 1998;144:441.
[43] Budzien J, McCoy JD, Rottach D, Curro JG. Polymer 2004;45:3923.